Please do not adjust margins

Journal Name

ARTICLE

Polyoxometalate-based metal-organic framework-derived hybrid electrocatalysts for highly efficient hydrogen evolution reaction

Ji-Sen Li,[a,b] Yu-Jia Tang,[a] Chun-Hui Liu,[a] Shun-Li Li,[a] Run-Han Li,[a] Long-Zhang Dong,[a] Zhi-Hui Dai,*[a] Jian-Chun Bao,[a] and Ya-Qian Lan*[a]

The design and fabrication of electrocatalysts for HER, with superior activity and stability, still remain significant challenge for clean and renewable energy technologies. Here we have synthesized Fe_3C/Mo_2C-containing N, P co-doped graphitic carbon derived from POM@MOF-100 (Fe) (denoted as $Fe_3C/Mo_2C@NPGC$) via a "killing three birds with one stone" strategy. The $Fe_3C/Mo_2C@NPGC$ catalyst demonstrates excellent electrocatalytic activity and stability towards HER with a low onset overpotential of 18 mV (vs. RHE), small Tafel slope of 45.2 mV dec^{-1}, as well as long-term durability for 10 h, which is one of the best non-noble metal HER catalysts in acidic media reported so far. Most importantly, this work opens up exciting opportunities for fabricating novel and highly efficient electrocatalysts to replace Pt or Pt-based catalysts utilizing POM-based metal-organic framework (MOF) as precursors.

Introduction

Global climate change and fossil fuel exhaustion have gained more attentions in recent years.[1] Hydrogen, produced via water splitting or hydrogen evolution reaction (HER), has been a research focus owing to its sufficient supply and lower environment pollution.[2,3] In this respect, the state-of-the-art HER catalysts are platinum (Pt) or Pt-based nanomaterials due to their low overpotential and fast kinetics for HER.[4,5] However, the high cost and low abundance of Pt, have severely restricted their practical and large-scale applications, further hampering the development of sustainable energy. Therefore, it is highly necessary to develop earth-abundant and low-cost electrocatalysts to replace Pt or Pt-based nanomaterials towards HER. To fulfill the dream, transition metal carbides (TMCs) or nitrides (TMNs), including Mo_2C, W_xC, Mo_xN, W_xN, etc., have been intensively investigated as outstanding catalysts for desulfurization,[6-8] reformation,[9-11] HER,[12-17] and so on,[18-20] due to their Pt-like behaviors.[21] Recently, post transition metals Fe,[22-24] Co,[25-26] and Ni,[27,28] doped Mo- and W-based catalysts have attracted tremendous attention because the dopant can tune their electronic states, increase their conductivity and explore more active sites. However, some problems such as the aggregation of nanoparticles, low density of active sites and so on,[17,23,29] still plague the material synthesis. Despite great efforts, the design

and synthesis of Fe, Co, and Ni doped Mo- and W-based HER electrocatalysts as alternatives to Pt, are still in their infant stage.

In terms of electrocatalysts for HER, porous carbon with large surface areas and porous structures are beneficial to the electrolyte diffusion and electron transport.[13,30] In particular, heteroatoms-doped porous carbon can be utilized as electrode materials,[31] or supports forming TMCs or TMNs-supported nanocomposites.[14,32] Based on the excellent electrochemistry performance of porous carbon materials, therefore, it is critical importance to develop new raw materials and method for the synthesis of carbon materials in electrochemical energy conversion systems. In recent years, as a new class of porous materials, metal–organic frameworks (MOFs),[33,34] have become a rapidly developing research area. Our group has paid attention to explore porous heteroatoms-doped carbon hybrids originating from MOFs as electrocatalysts for oxygen reduction reaction (ORR),[35,36] while the dopant of heteroatoms, offering more active sites, can enhance their catalytic performance.[37] In addtition, polyoxometalate (POM)-based MOFs combining the advantages of both POMs and MOFs,[38-41] have received great interest because they may offer not only organic ligands with regular arrangement but also Mo, W etc. sources, which contribute to the synthesis of porous carbon supported Mo-, and W-based electrocatalysts with large surface areas by carbonization.[42,43]

Considering the above, if we synthesize POM-based Fe-MOFs by combining Fe-based MOFs and POMs, then we can use them as precursors to achieve iron carbide or nitride doped porous carbon supported Mo- and W-based electrocatalysts, which are almost impossible to achieve via a single MOFs precursor. More importantly, owing to the confinement effect of porous MOFs, these obtained metal

a. *School of Chemistry and Materials Science, Nanjing Normal University, Nanjing 210023, P. R. China*
b. *Key Laboratory of Inorganic Chemistry in Universities of Shandong, Department of Chemistry and Chemical Engineering, Jining University, Qufu, 273155, Shandong, P. R. China.*

nanoparticles may be small-sized, homogeneously embedded in carbon matrix without aggregation with high denstiy. As well, because of the existence of Fe,[35] the graphitic degrees of electrocatalysts also can be significantly enchanced. As a consequence, we predict that the fabrication of novel catalysts derived from POM-based MOFs is at the forefront of research for energy storage and conversion system. To the best of our knowledge, iron carbide or nitride doped porous carbon supported Mo-, and W-based electrocatalysts using MOFs as precursors by a facile approach remain largely unexplored to date.

Herein, for the first time, we conceived a novel approach for the fabrication of Fe_3C/Mo_2C-containing N, P co-doped graphitic carbon (designated as $Fe_3C/Mo_2C@NPGC$) utilizing $PMo_{12}@MIL$-100 (Fe) as precursors, which provide Fe, Mo and P sources simultaneously. This method reduces the number of synthetic procedures and energy consumption. Most importantly, hierarchically structured porous carbons can be obtained from MOFs, and the existence of Fe derived from MIL-100 (Fe) is beneficial to forming the highly graphitized carbon. By the ingenious "killing three birds with one stone" synthesis, the resultant $Fe_3C/Mo_2C@NPGC$ catalyst has three prominent characteristics as follows: (1) nano-sized Fe_3C/Mo_2C nanoparticles, which are uniformly encased in graphitic carbon; (2) mesoporous structures; (3) N, P co-doped graphitic carbon. As we expected, taking the advantage of the aforementioned superiority, the catalyst shows excellent electrocatalytic activity and stability towards HER, which is one of the best non-noble metal HER catalysts in acidic media reported so far.

Results and discussion

MIL-100 (Fe) and $PMo_{12}@MIL$-100 (Fe) were synthesized according to a previous report,[44] and the corresponding morphologies and structures were characterized by transmission electron microscopy (TEM) and powder X-Ray diffraction (PXRD). As revealed in Fig. S1, the TEM images of MIL-100 (Fe) and $PMo_{12}@MIL$-100 (Fe) display the polyhedral morphologies. The corresponding PXRD patterns match well with that of the simulated crystals (Fig. S2), confirming the phase purity and good crystallinity.[45] Additionally, the results also prove that the framework structures remain still intact after the incorporation of PMo_{12}. Subsequently, the
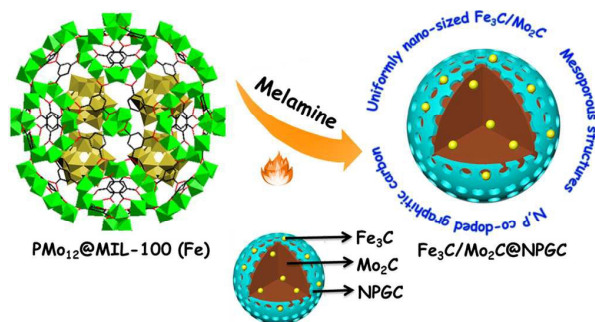
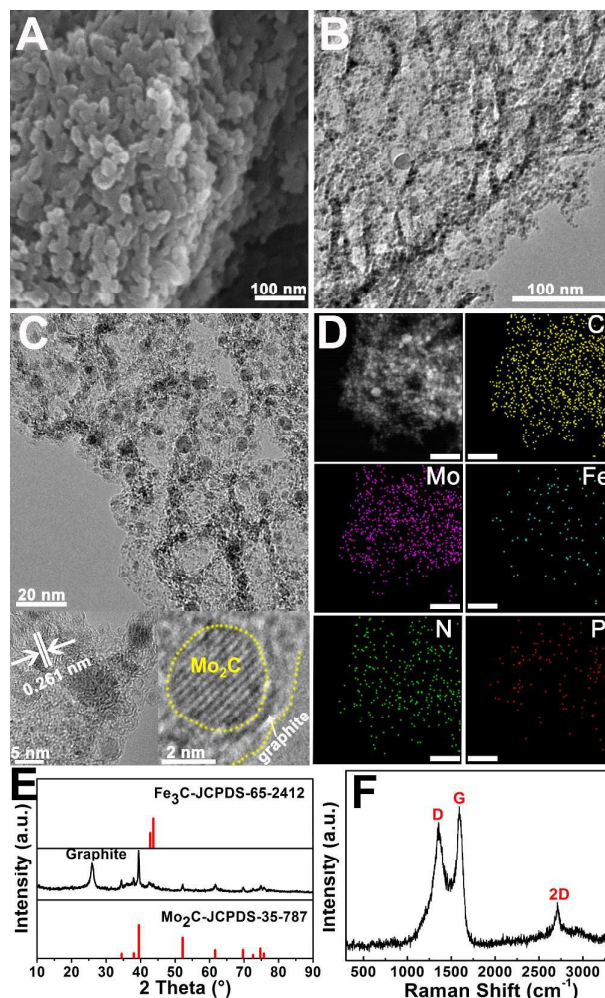Scheme 1 Preparation of $Fe_3C/Mo_2C@NPGC$ nanocomposite derived from POM-based MOFs.

Fig. 1 Typical SEM image (A), low (B) and high magnification TEM images (C), STEM image and EDS elemental mapping of C, Mo, Fe, N, and P, (D), scale bar 50 nm, EDS spectroscopy (E), PXRD pattern (F), and Raman spectroscopy (G) of $Fe_3C/Mo_2C@NPGC$.

$Fe_3C/Mo_2C@NPGC$ catalyst was obtained by carbonizing the mixture of $PMo_{12}@MIL$-100 (Fe) and melamine at 900 °C in N_2 atmosphere (Scheme 1). For comparison, the $Fe_3C@C$ and $Fe_3C/FeMo/Mo_2C$ catalysts were also prepared via the carbonization of sole MIL-100 (Fe) or $PMo_{12}@MIL$-100 (Fe) under identical condition, respectively.

As seen from Fig. 1A-C, scanning electron microscope (SEM) and TEM images of $Fe_3C/Mo_2C@NPGC$ suggest that the porous feature of the resulted carbon materials. The large amount of nano-sized Fe_3C/Mo_2C nanoparticles is uniformly decorated on the resultant porous carbon. The high-resolution TEM (HRTEM) image of $Fe_3C/Mo_2C@NPGC$ (Fig. 1C) shows the obvious lattice fringes with an interplanar distance of 0.261 nm, corresponding to the (100) plane of Mo_2C. Surprisingly, it is found that the Mo_2C nanoparticle is coated with uniform graphitic carbon layers, which effectively prevent Mo_2C particles from aggregating and benefit the fast electron transfer.[46,47] Fig. 1D demonstrates that the scanning TEM (STEM) and corresponding energy dispersive X-ray

spectroscopy (EDS) elemental mapping images of Fe$_3$C/Mo$_2$C@NPGC, which reveal that C, Mo, Fe, N, and P elements are distributed on the Fe$_3$C/Mo$_2$C@NPGC surface, consistent with the EDS spectrum (Fig. 1E).

The phase of Fe$_3$C/Mo$_2$C@NPGC was further analyzed by PXRD, illustrated in Fig. 1F. The peaks located at 34.5, 38.04, 39.56, 52.2, 61.62, 69.72, 72.6, 74.74, and 75.74° are clearly observed, indexed to (100), (002), (101), (102), (110), (103), (200), (112), and (201) planes of Mo$_2$C, respectively (JCPDS, No. 35-787). The peaks around 42.86, and 43.78° correspond to (011) and (002) planes of Fe$_3$C (JCPDS, No. 65-2412), and the additional peak observed at 26° is stemmed from graphitic carbon. To further verify the structural information, Raman spectroscopy is used to characterize Fe$_3$C/Mo$_2$C@NPGC. Generally, two peaks at about 1350 and 1598 cm^{-2} correspond to the D and G band, attributed to disordered carbon, and ordered graphitic carbon, respectively. The other peak at about 2700 cm^{-2} is assigned to 2D band.[48] The intensity ratio between G and D bands (I_G/I_D) is a parameter of graphitic degree of carbon materials. In terms of Fe$_3$C/Mo$_2$C@NPGC, the value of I_G/I_D is 0.81, suggesting the high graphitic degree (Fig. 1G).

For comparison, the morphologies and structures of Fe$_3$C@C and Fe$_3$C/FeMo/Mo$_2$C were also investigated by SEM, TEM, HRTEM, element mapping, EDS, PXRD, and Raman spectroscopy (Fig. S3 and Fig. S4). For Fe$_3$C@C, it is found that only a negligible amount of Fe$_3$C are encased in the carbon shell, and the graphitic degree is lower than that of Fe$_3$C/Mo$_2$C@NPGC. Whereas, in terms of Fe$_3$C/FeMo/Mo$_2$C, it is surprisingly found that nanoparticles are severely aggregated together and no porous carbon is existent. We speculate that it is possibly related to the shortage of carbon sources derived from MOFs because partial carbons were consumed by the oxygen of PMo$_{12}$ during the carbonization process. Thus, the existence of melamine plays crucial roles in the provision of carbon and nitrogen sources.

The N$_2$ adsorption-desorption isotherms and pore size distributions of Fe$_3$C@C, Fe$_3$C/FeMo/Mo$_2$C, and Fe$_3$C/Mo$_2$C@NPGC are displayed in Fig. S5, respectively. As seen from these isotherms, the hysteresis can be clearly observed, characteristic of meso-porous structures.[48] The Brunauer–Emmett–Teller (BET) specific surface area of Fe$_3$C/Mo$_2$C@NPGC is 128 m^2 g^{-1}, which is higher than that of Fe$_3$C/FeMo/Mo$_2$C (40 m^2 g^{-1}), and lower than that of Fe$_3$C@C (470 m^2 g^{-1}). Based on the Barrett–Joyner–Halenda (BJH) model, the corresponding pore size distributions are mainly centered at about 2.5 and 4 nm, suggesting the existence of mesopores. The active surface areas, and mesoporous structures can accelerate the interfacial electrocatalytic reactions and charge transfer, further boosting the HER activity.[49]

To further determine the elemental compositions and valence states of Fe$_3$C/Mo$_2$C@NPGC, X-ray photon spectroscopy (XPS) were performed. As depicted in Fig. 2A, the elements of C, P, Mo, N, and Fe can be obviously identified. The high-resolution XPS spectrum of C1s (Fig. 2B) can be
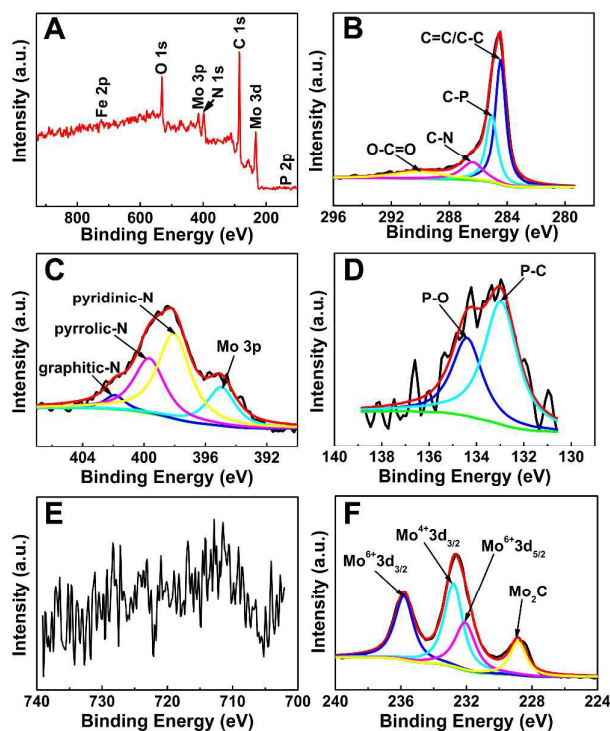

Fig. 2 XPS survey spectra (A) and high-resolution scans of (B) C 1s, (C) N 1s, (D) P 2p, (E) Fe 2p, and (F) Mo 3d electrons of Fe$_3$C/Mo$_2$C@NPGC.

ascribed to C-C/C=C(284.6 eV), C-P (285.1 eV), C-N (286.1 eV), and O-C=O (289.8 eV), respectively.[12,37] Fig. 2C shows high-resolution N 1s XPS peaks are fitted into three peaks, assigned to pyridinic-N (397.9 eV), pyrrolic-N (399.5 eV), and graphitic-N (401.7 eV), respectively.[46,47] In general, graphitic and pyridinic-N are more active than the pyrrolic-N, beneficial to enhancing catalytic activity. The high resolution P 2p peaks are also deconvoluted into P-C (132.9 eV) and P-O (134.3 eV), which originates from surface oxidation owing to air contact (Fig. 2D).[12,50] Meanwhile, the P-C bonds indicate that the electrons in P have been doped into carbon. In terms of Fe 2p (Fig. 2E), the signal is very weak and the content is just 0.42% under the XPS detection limit (< 1 at. %), further implying that most of iron carbide nanoparticles were encapsulated in the graphitic carbon layers. Additionally, Fig. 2F exhibits the high resolution Mo 3d XPS. These peaks at 232.05, 235.2, and 232.7 eV are attributed to MoO$_3$, and MoO$_2$ due to surface oxidation. The other peak at 228.8 eV is assigned to Mo^{2+}, arising from Mo$_2$C.[13,46] In Figure S6, the O 1s peaks at 530.2, 530.9, 531.7, and 532.5 eV, are assigned to Mo-O, C=O/P-O, P=O, and C-O, respectively.

For comparison, the high-resolution XPS analyses of Fe$_3$C@C, and Fe$_3$C/FeMo/Mo$_2$C are also used to estimate their surface elemental contents. The characteristic peaks of C 1s, Fe 2p, and Mo 3d are shown in Fig. S7-8, respectively. The corresponding element contents are listed in Table S1.

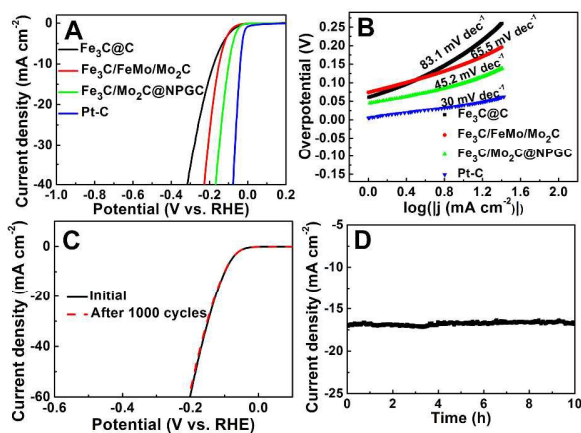The electrocatalytic HER activity of Fe$_3$C/Mo$_2$C@NPGC was evaluated using a typical three- electrode system in 0.5 M

Fig. 3 (A) Polarization curves of different samples. (B) Corresponding Tafel plots of the polarization curves. (C) Polarization curves of Fe$_3$C/Mo$_2$C@NPGC initially and after 1000 cycles. (D) Time dependence of current density under static overpotential of 120 mV for 10 h.

H$_2$SO$_4$ electrolyte. Fe$_3$C@C, Fe$_3$C/FeMo/Mo$_2$C and 20% Pt-C were also assessed for comparison. All potentials are given in the work with respect to the reversible hydrogen electrode (RHE). Fig. 3A shows the corresponding polarization curves without IR compensation. As well-known, Pt-C shows a high HER activity with nearly zero onset overpotential.[14,42] It is surprising that Fe$_3$C/Mo$_2$C@NPGC exhibits a small onset overpotential of 18 mV, much lower than those of Fe$_3$C@C (43 mV), Fe$_3$C/FeMo/Mo$_2$C (44 mV), and even comparable to that of Pt-C. Moreover, when the overpotential is beyond 18 mV, the cathodic current rises rapidly with more negative potential. Generally, the overpotential at current density of 10 mA cm^{-2} is an important reference point.[5] To attain the value, Fe$_3$C@C, and Fe$_3$C/FeMo/Mo$_2$C need overpotential of 175, and 150 mV, whereas Fe$_3$C/Mo$_2$C@NPGC only requires an overpotential of 98 mV, further suggesting excellent HER activity of Fe$_3$C/Mo$_2$C@NPGC. These values of Fe$_3$C/Mo$_2$C@NPGC catalyst are comparable favorably with, even superior to the other reported non-noble metal catalysts for HER in acidic media (Table S2).

Generally speaking, Tafel slope is also a crucial parameter for the kinetic activity of electrodes, which is exhibited in Fig. 3B. The value of Tafel slope for Fe$_3$C/Mo$_2$C@NPGC is 45.2 mV dec^{-1}, which is much lower than those of Fe$_3$C@C (83.1 mV dec^{-1}) and Fe$_3$C/FeMo/Mo$_2$C (65.5 mV dec^{-1}), comparable to that of Pt-C (30 mV dec^{-1}). Hence, we believe that the HER for Fe$_3$C/Mo$_2$C@NPGC possibly proceeds by a Volmer-Heyrovsky mechanism, implying that electrochemical desorption is the rate-limiting step.[3,52] The exchange current density (j_0) is calculated according to the corresponding Tafel plots by extrapolation methods, shown in Fig. S9. The j_0 of 1.04×10^{-4} A cm^{-2} for Fe$_3$C/Mo$_2$C@NPGC is superior to that of Fe$_3$C/FeMo/Mo$_2$C (0.75×10^{-4} A cm^{-2}), and slightly lower than those of Fe$_3$C@C (1.81×10^{-4} A cm^{-2}), and Pt-C (3.92×10^{-4} A cm^{-2}), further demonstrating the favorable HER kinetics at the Fe$_3$C/Mo$_2$C@NPGC/electrolyte interface, which is one of the

largest values among the reported Mo$_2$C catalysts so far (Table S2).

To gain additional insight into HER, the electrochemical surface areas (ECSA) of different catalysts were measured by the double-layer capacitance (C$_{dl}$). The cyclic voltammograms (CVs) were performed in the region of 0.19-0.39 V at different scan rates (Fig. S10). The C$_{dl}$ of Fe$_3$C@C, Fe$_3$C/FeMo/Mo$_2$C, and Fe$_3$C/Mo$_2$C@NPGC are 8.47, 5.17, and 5.74 mF cm^{-2}, respectively. Furthermore, we further inspect the activities of three catalysts using an electrochemical impedance spectroscopy (EIS) technique. The charge-transfer resistance (R$_{ct}$) stems from high frequencies in Nyquist plot. In other words, lower value corresponds to faster HER kinetics. Compared to Fe$_3$C@C (0.3 Ω), the R$_{ct}$ of Fe$_3$C/Mo$_2$C@NPGC (6.2 Ω) is larger, but more lower than Fe$_3$C/FeMo/Mo$_2$C (3385 Ω), implying that Fe$_3$C/Mo$_2$C@NPGC possesses better electron transfer ability (Fig. S11). Considering the above results, we infer that the contact area is not sole factor for electrocatalytic activity towards HER. On the contrary, the structure, size, and amount of active sites may be major causes of different activities.

Stability is another crucial criterion for HER catalysts. To assess the durability of the Fe$_3$C/Mo$_2$C@NPGC catalyst, a long-term cycling test between -0.3 and 0.3 V was carried out at the scan rate of 100 mV s^{-1}. After 1000 cycles, the polarization curve for Fe$_3$C/Mo$_2$C@NPGC is almost identical to the initial one (Fig. 3C). In addition, to further probe the electrochemical stability, the continuous HER at constant overpotential was also performed. Fig. 3D presents the current density at the overpotential of 120 mV for 10 h maintains negligible changes. These results effectively highlight the remarkable stability of the Fe$_3$C/Mo$_2$C@NPGC catalyst in acidic solution. This is associated with the existence of carbon shells, which protect Fe$_3$C/Mo$_2$C against air oxidation and enhance electron penetration.[47,53]

Based on the above-mentioned, the excellent eletrcocatalytic activity can be explained as follows: 1) because of the dopant of heteroatoms (N, P), the electroneutrality is broken and the electronic structure of C atom is changed, further increasing the number of active sites.[37,48,52] Meanwhile the Gibbs free energy of proton adsorption-desorption is lowered, contributing to a synergistically improved HER performance. 2) the small size of Mo$_2$C in the catalyst is beneficial to providing more exposed active sites.[41] Experimental and theoretical investigations have demonstrated that the electronic structure of catalyst could be changed with the incorporation of transition-metal, further boosting the HER activity.[24,27,47] Furthermore, the existence of graphitic carbon layers not only hampers the aggregation and surface oxidation of Fe$_3$C/Mo$_2$C nanoparticles, but also promotes electron penetration from Fe$_3$C/Mo$_2$C to the graphitic carbon surface.[47,53] Last but not the least, the geometric confinement of Fe$_3$C/Mo$_2$C inside carbon layers can also improve the catalytic activity for HER.[42,53] 3) the porous structures of Fe$_3$C/Mo$_2$C@NPGC provide efficient pathways for mass transport and improve the electrical conductivity.[32,49] Overall, originating from the synergistic effects of these above
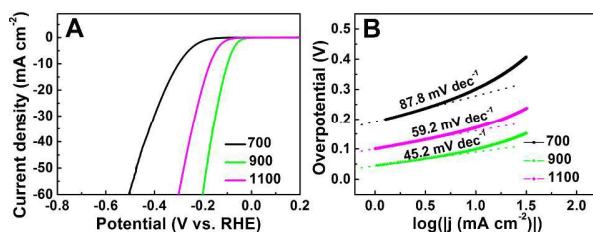
Fig. 4 (A) Polarization curves of $Fe_3C/Mo_2C@NPGC$ carbonized at 700, 900, and 1100 ^oC, respectively. (B) Corresponding Tafel plots of A.

factors, the $Fe_3C/Mo_2C@NPGC$ catalyst shows outstanding HER activity.

In control experiment, to investigate the influence of carbonization temperature on the HER, the mixture of $PMo_{12}@MIL-100$ (Fe) and melamine was carbonized at 700 and 1100 ^oC (defined as $Fe_3C/Mo_2C@NPGC-700$, and $Fe_3C/Mo_2C@NPGC-1100$), respectively. The morphologies and structures were also evaluated in detail (Fig. S12-17). And then, the HER activities of different catalysts were examined by the same measurements. As seen from Fig. 4A, the electrocatalytic activity of $Fe_3C/Mo_2C@NPGC-700$, 1100, 900 increases sequentially. Tafel slopes of $Fe_3C/Mo_2C@NPGC-700$, 900, 1100 are calculated to be 87.8, 45.2, and 59.2 mV dec^{-1}, respectively (Fig. 4B). Overall, among the three catalysts, $Fe_3C/Mo_2C@NPGC-900$ exhibits the best electrocatalytic activity for HER, which may be related to the amount of heteroatoms (N, and P) and sizes of nanoparticles. That is, high carbonization temperature results in sintering and aggregating of Fe_3C/Mo_2C nanoparticles, which reduces the number of exposed active sites. Simultaneously, the contents of heteroatoms (N, and P) obviously decrease (Table S1), implying the loss of active sites.

Conclusions

In summary, we have fabricated novel and highly efficient $Fe_3C/Mo_2C@NPGC$ catalyst based on $PMo_{12}@MIL-100$ (Fe) by in-situ approach for the first time. The "killing three birds with one stone" strategy endows this catalyst with three features: nano-sized nanoparticles, mesopores, N, P co-doped graphitic carbon. The synthesized $Fe_3C/Mo_2C@NPGC$ catalyst exhibits prominent electrocatalytic activity: the onset overpotential is 18 mV, Tafel slope is 45.2 mV dec^{-1}, and long-time durability is more than 10 h, which is one of the best non-noble metal HER catalysts in acidic media reported so far. Therefore, our work here not only provides us a novel and low-cost electrocatalyst with excellent activity towards HER, but also opens up new avenues for the design and fabrication of nanomaterials derived from POM-based MOFs for HER, ORR, and battery applications.

Acknowledgements

Notes and references

1   J. A. Turner, *Science,* 2004, **305**, 972-974.
2   J. R. McKone, S. C. Marinescu, B. S. Brunschwig, J. R. Winkler and H. B. Gray, *Chem. Sci.*, 2014, **5**, 865-878.
3   C. G. Morales-Guio, L.-A. Stern and X Hu, *Chem. Soc. Rev.,* 2014, **43**, 6555-6569.
4   V. R. Stamenkovic, B. S. Mun, M. Arenz, K. J. J. Mayrhofer, C. A. Lucas, G. Wang, P. N. Ross and N. M Markovic, *Nat. Mater.,* 2007, **6**, 241-247.
5   M. G. Walter, E. L. Warren, J. R. McKone, S. W. Boettcher, Q. Mi, E. A. Santori and N. S. Lewis, *Chem. Rev.,* 2010, **110**, 6446-6473.
6   T. G. Kelly and J. G. Chen, *Chem. Soc. Rev.,* 2012, **41**, 8021-8034.
7   A. Szymańska-Kolasa, M. Lewandowski, C. Sayag and G. Djéga-Mariadassou, *Catal. Today,* 2007, **119**, 7-12.
8   L. Coulier, G. Kishan, J. A. R. van Veen and J. W. Niemantsverdriet, *J. Phys. Chem. B,* 2002, **106**, 5897-5906.
9   N. M. Schweitzer, J. A. Schaidle, O. K. Ezekoye, X. Pan, S. Linic and L. T. Thompson, *J. Am. Chem. Soc.,* 2011, **133**, 2378-2381.
10 N. Ji, T. Zhang, M. Zheng, A. Wang, H. Wang, X. Wang and J. G. Chen, *Angew. Chem. Int. Ed.,* 2008, **47**, 8510-8513.
11 W.-S. Lee, Z. Wang, R. J. Wu and A. Bhan, *J. Catal.,* 2014, **319**, 44-53.
12 H. Yan, C. Tian, L. Wang, A. Wu, M. Meng, L. Zhao and H. Fu, *Angew. Chem. Int. Ed.,* 2015, **54**, 6325-6329.
13 Y. Zhao, K. Kamiya, K. Hashimoto and S. Nakanishi, *J. Am. Chem. Soc.,* 2015, **137**, 110-113.
14 D. H. Youn, S. Han, J. Y. Kim, J. Y. Kim, H. Park, S. H. Choi and J. S. Lee, *ACS Nano,* 2014, **8**, 5164-5173.
15 C. Wan, Y. N. Regmi and B. M. Leonard, *Angew. Chem. Int. Ed.,* 2014, **53**, 6407-6410.
16 W.-F. Chen, S. Iyer, S. Iyer, K. Sasaki, C.-H. Wang, Y. Zhu, J. T. Muckerman and E. Fujita, *Energy Environ. Sci.,* 2013, **6**, 1818-1826.
17 H. Vrubel and X. Hu, *Angew. Chem. Int. Ed.,* 2012, **51**, 12703-12706.
18 H.-J. Zhang, K.-X. Wang, X.-Y. Wu, Y.-M. Jiang, Y.-B. Zhai, C. Wang, X. Wei and J.-S. Chen, *Adv. Funct. Mater.,* 2014, **24**, 3399-3404.
19 M. D. Porosoff, X. Yang, J. A. Boscoboinik and J. G. Chen, *Angew. Chem. Int. Ed.,* 2014, **53**, 6705-6709.
20 W. Zheng, T. P. Cotter, P. Kaghazchi, T. Jacob, B. Frank, K. Schlichte, W. Zhang, D. S. Su, F. Schüth and R. Schlögl, *J. Am. Chem. Soc.,* 2013, **135**, 3458-3464.
21 R. B. Levy and M. Boudart, *Science,* 1973, **181**, 547-549.
22 D. Merki, H. Vrubel, L. Rovelli, S. Fierro and X. Hu, *Chem. Sci.,* 2012, **3**, 2515-2525.
23 Y. Zhao, K. Kamiya, K. Hashimoto and S. Nakanishi, *Angew. Chem. Int. Ed.,* 2013, **52**, 13638-13641.
24 C. Wan and B. M. Leonard, *Chem. Mater.,* **2015**, *27*, 4281-4288.

25 B. Cao, G. M. Veith, J. C. Neuefeind, R. R. Adzic and P. G. Khalifah, *J. Am. Chem. Soc.,* 2013, 135, 19186-19192.

26 P. D. Tran, S. Y. Chiam, P. P. Boix, Y. Ren, S. S. Pramana, J. Fize, V. Artero and J. Barber, *Energy Environ. Sci.,* 2013, **6**, 2452-2459.

27 W.-F. Chen, K. Sasaki, C. Ma, A. I. Frenkel, N. Marinkovic, J. T. Muckerman, Y. Zhu and R. R. Adzic, *Angew. Chem. Int. Ed.,* 2012, **51**, 6131-6135.

28 Y. Ma, G. Guan, P. Phanthong, X. Hao, W. Huang, A. Tsutsumi, K. Kusakabe and A. Abudula, *J. Phys. Chem. C,* 2014, **118**, 9485-9496.

29 S. Wang, X. Yu, Z. Lin, R. Zhang, D. He, J. Qin, J. Zhu, J. Han, L. Wang, H.-k. Mao, J. Zhang and Y. Zhao, *Chem. Mater.,* 2012, **24**, 3023-3028.

30 K. Xiong, L. Li, L. Zhang, W. Ding, L. Peng, Y. Wang, S. Chen, S. Tan, Z. Wei, *J. Mater. Chem. A,* 2015, **3**, 1863-1867.

31 J. Duan, S. Chen, M. Jaroniec and S. Z. Qiao, *ACS Nano*, 2015, **9**, 931-940.

32 R. Wu, J. Zhang, Y. Shi, D. Liu and B. Zhang, *J. Am. Chem. Soc.,* 2015, 137, 6983-6986.

33 S.-L. Li and Q. Xu, *Energy Environ. Sci.,* 2013, **6**, 1656-1683.

34 H.-C. Zhou, J. R Long, and O. M. Yaghi, *Chem. Rev.,* 2012, **112**, 673-674.

35 J.-S. Li, S.-L. Li, Y.-J. Tang, M. Han, Z.-H. Dai, J.-C. Bao and Y.-Q. Lan, *Chem. Commun.,* 2015, **51**, 2710-2713.

36 J.-S. Li, S.-L. Li, Y.-J. Tang, K. Li, L. Zhou, N. Kong, Y.-Q. Lan, J.-C. Bao and Z.-H. Dai, *Sci. Rep.,* 2014, **4***, 5130*.

37 W. Ai, Z. Luo, J. Jiang, J. Zhu, Z. Du, Z. Fan, L. Xie, H. Zhang, W. Huang and T. Yu, *Adv. Mater.,* 2014, **26**, 6186-6192.

38 D.-Y. Du, J.-S. Qin, S.-L. Li, Z.-M. Su and Y.-Q. Lan, *Chem. Soc. Rev.,* 2014, **43**, 4615-4632.

39 A. Dolbecq, E. Dumas, C. R. Mayer and P. Mialane, *Chem. Rev.,* 2010, **110**, 6009-6048.

40 S.-S. Wang and G.-Y Yang, *Chem. Rev.,* 2015, **115**, 4893-4962.

41 J.-S. Qin, D.-Y. Du, W. Guan, X.-J. Bo, Y.-F. Li, L.-P. Guo, Z.-M. Su, Y.-Y. Wang, Y.-Q. Lan and H.-C. Zhou, *J. Am. Chem. Soc.,* 2015, **137**, 7169-7177.

42 H. B. Wu, B. Y. Xia, L. Yu, X.-Y. Yu and X. W. Lou, *Nat. Commun.,* 2015, **6***, 6512.

43 Y.-J. Tang, M.-R. Gao, C.-H Liu, H.-L. Jiang, Y.-Q. Lan, Min Han and S.-H. Yu, *Angew. Chem. Int. Ed.,* 2015, **54**, DOI: 10.1002/anie.201505691.

44 R. Canioni, C. Roch-Marchal, F. Secheresse, P. Horcajada, C. Serre, M. Hardi-Dan, G. Ferey, J.-M. Greneche, F. Lefebvre, J.-S. Chang, Y.-K. Hwang, O. Lebedev, S. Turner and G. Van Tendeloo, *J. Mater. Chem.,* 2011, **21**, 1226-1233.

45 G. Férey, C. Serre, C. Mellot-Draznieks, F. Millange, S. Surblé, J. Dutour and I. Margiolaki, *Angew. Chem. Int. Ed.,* 2004, **43**, 6296-6301.

46 Y. Liu, G. Yu, G.-D. Li, Y. Sun, T. Asefa, W. Chen and X. Zou, *Angew. Chem. Int. Ed.,* 2015, **54**, DOI: 10.1002/anie.201504376.

47 W. Zhou, J. Zhou, Y. Zhou, J. Lu, K. Zhou, L. Yang, Z. Tang, L. Li and S. Chen, *Chem. Mater.,* 2015, **27**, 2026-2032.

48 J. Liang, Y. Jiao, M. Jaroniec and S. Z. Qiao, *Angew. Chem. Int. Ed.,* 2012, **51**, 11496-11500.

49 L. Liao, S. Wang, J. Xiao, X. Bian, Y. Zhang, M. D. Scanlon, X. Hu, Y. Tang, B. Liu and H. H. Girault, *Energy Environ. Sci.,* 2014, 7, 387-392.

50 J. Duan, S. Chen, B. A. Chambers, G. G. Andersson and S. Z. Qiao, *Adv. Mater.,* 2015, **27**, 4234-4241.

51 D. Deng, L. Yu, X. Chen, G. Wang, L. Jin, X. Pan, J. Deng, G. Sun and X. Bao, *Angew. Chem. Int. Ed.,* 2013, **52**, 371-375.

52 Y. Zheng, Y. Jiao, M. Jaroniec and S. Z. Qiao, *Angew. Chem. Int. Ed.,* 2015, **54**, 52-65.

53 J. Deng, P. Ren, D. Deng and X. Bao, *Angew. Chem. Int. Ed.,* 2015, **54**, 2100-2104.

Graphical abstract

Polyoxometalate-based metal-organic framework-derived hybrid electrocatalysts for highly efficient hydrogen evolution reaction

Ji-Sen Li, Yu-Jia Tang, Chun-Hui Liu, Shun-Li Li, Run-Han Li, Long-Zhang Dong, Zhi-Hui Dai,* Jian-Chun Bao, and Ya-Qian Lan*

Novel Fe_3C/Mo_2C-containing N, P co-doped graphitic carbon derived from POM@MOF-100 (Fe) has been synthesized *via* a "killing three birds with one stone" strategy for the first time. The nanomaterial demonstrates a low onset overpotential of 18 mV (vs. RHE), small Tafel slope of 45.2 mV dec^{-1}, as well as long-term durability for 10 h, which is one of the best non-noble metal HER catalysts in acidic media reported so far.